

Rapid late Miocene rise of the Bolivian Altiplano: Evidence for removal of mantle lithosphere

Carmala N. Garzione^{a,b,*}, Peter Molnar^b, Julie C. Libarkin^c, Bruce J. MacFadden^d

^a Department of Earth and Environmental Sciences, University of Rochester, Rochester, NY 14627, U.S.A.

^b Department of Geological Sciences and Cooperative Institute for Research in Environmental Science, University of Colorado, Boulder, CO 80309, U.S.A.

^c Department of Geological Sciences, Ohio University, Athens, OH 45701, U.S.A.

^d Florida Museum of Natural History, University of Florida, Gainesville, FL 32611, U.S.A.

Received 11 August 2005; received in revised form 16 November 2005; accepted 17 November 2005

Available online 27 December 2005

Editor: Scott King

Abstract

The oxygen isotopic compositions of carbonates deposited in the northern Altiplano demonstrate a rapid change in late Miocene time, which we attribute to an increase in elevation. Rainfall samples over an elevation transect adjacent to the Altiplano of northern Bolivia display a systematic decrease in mean annual $\delta^{18}\text{O}$ values and define a local $\delta^{18}\text{O}$ vs. altitude gradient [R. Gonfiantini, M.-A. Roche, J.-C. Olivry, J.-C. Fontes, G.M. Zuppi, The altitude effect on the isotopic composition of tropical rains, *Chem. Geol.* 181 (2001) 147–167.], which we apply to paleo-meteoric water values determined from carbonates. Age constraints from magnetostratigraphy and paleoelevation estimates suggest surface uplift of ~2.5 to 3.5 km occurred between ~10.3 Ma and 6.8 ± 0.4 Ma, when the Altiplano rose to its current elevation. Only the removal of dense eclogitic lower crust and mantle lithosphere can generate a change of this magnitude and rapidity. This change coincides with an ~30% decrease in the rate of convergence between the South America and Nazca plates and the propagation of deformation into the eastern Subandean zone, which we infer to have resulted from the increase in the force per unit length applied by the elevated Andean plateau to the surrounding lowlands.

© 2005 Elsevier B.V. All rights reserved.

Keywords: Altiplano; paleoelevation; oxygen isotopes; lithosphere removal

1. Introduction

The amount and timing of regional elevation change can place crucial constraints on the geodynamic processes responsible for the formation of high plateaus in contractional mountain belts. Surface uplift of thousands of meters over a vast region results from redis-

tribution of mass at depth and consequent isostatic compensation, with two classes of processes accounting for most redistribution: thickening of the relatively light crust and removal of relatively dense mantle lithosphere [2,3]. Moreover, removal of especially dense eclogite, formed in the lower crust in regions of crustal thickening, can greatly enhance the resulting elevation change [4–9]. Depending upon the amount and depth range over which mass is redistributed, the force per unit length that a high terrain applies to surrounding lowlands can change sufficiently to resist continued con-

* Corresponding author. Department of Earth and Environmental Sciences, University of Rochester, Rochester, NY 14627, U.S.A.
E-mail address: garzione@earth.rochester.edu (C.N. Garzione).

vergence between adjacent plates and transform the style of deformation from crustal shortening and thickening to crustal extension and thinning [10]. Although numerous proposals have been made for the role played by the mantle beneath mountain belts, tests of them remain few, and the history of paleoelevations offers one possible test. This study provides paleoelevation evidence from the central Andes, a region where extensive previous work demonstrates both thick crust and a relatively hot upper mantle, and where the relative roles of crustal thickening and of removal of mantle lithosphere, including eclogite, have been addressed using a variety of observations.

2. Geologic background

Situated in the central Andes, the Altiplano forms a plateau of a moderate topography over a width of ~200 km and at a mean elevation of 3.8 km (Fig. 1). The gentle landscape of the Altiplano has resulted, in part, from internal drainage since late Oligocene time [11,12]. As parts of the Andean plateau, the Western and Eastern Cordillera flank both sides of the Altiplano and reach peak elevations exceeding 6 km. The Western Cordillera is the active magmatic arc and is marked by a string of stratovolcanoes, whereas the Eastern Cordillera is a fold-thrust belt formed in early Paleozoic metasedimentary rock (Fig. 1). Provenance and paleocurrent data from sedimentary rock in the eastern Altiplano basin indicate a late Oligocene

minimum age of initial shortening in the Eastern Cordillera [11,13]. Shortening had largely ceased in the Altiplano and western part of the Eastern Cordillera by early Miocene time as evidenced by only minor deformation of overlying late Oligocene to early Miocene deposits [14–16]. Basement-involved thrusting in the Interandean zone likely occurred after the cessation of deformation in the Eastern Cordillera, although estimates of the initial timing of thrusting range from early Miocene [16] to late Miocene time [17]. Minor folding and thrusting continued in the Altiplano until late Miocene time and produced ~30 km of additional shortening [18]. The Subandean zone became active during late Miocene time [19–21] and currently accommodates most of the shortening across the Central Andes [22].

The surface manifestations of various lithospheric processes led previous workers to propose that the Altiplano rose to its present elevation in two stages [19,23,24]. The 70–60 Ma El Molino Formation, containing shallow marine deposits, requires that the Altiplano lay at sea level at the end of the Cretaceous [25]. The early rise of the Andes, prior to 10 Ma, is thought to be associated with upper crustal shortening as recorded by the temporal evolution of the Andean fold-thrust belt and synorogenic sedimentation [13,16,23].

Geomorphological observations have been used to infer surface uplift of kilometers since 10 Ma. Widespread, low-relief paleosurfaces across the eastern Cordillera reflect the remnants of low relief drainage systems that flowed toward the Amazon foreland and are thought to have formed at low elevation [19,24]. Tuffs that mantle and/or are cut by these surfaces place upper bounds of ~7 to 12 Ma on the age of the surfaces [24]. Tuffs that overlie drainages that dissect the paleosurface indicate that widespread incision began between ~6.5 and 3 Ma, and reconstructions of the relief in these drainages have been used to infer ~2 km of downcutting below the paleosurfaces [24].

Prior to our study, the only estimates of Andean paleoelevations relied on leaf physiognomy, interpreted to indicate an elevation of no more than a third of its modern average height of 3800 m at ~15 to 20 Ma and no more than half by ~10 Ma [26]. In particular, from paleotemperature estimates of $18.6 \pm 21.0 \pm 2.1$ °C for the 10.66 ± 0.06 Ma Jakokkota flora (modern elev. = 4300 m) in the northwestern Altiplano (Fig. 1), Gregory-Wodzicki [27] inferred that the flora grew between elevations of 590 and 1610 ± 1000 m.

Geophysical constraints on deep structure are consistent with removal of mantle lithosphere and perhaps

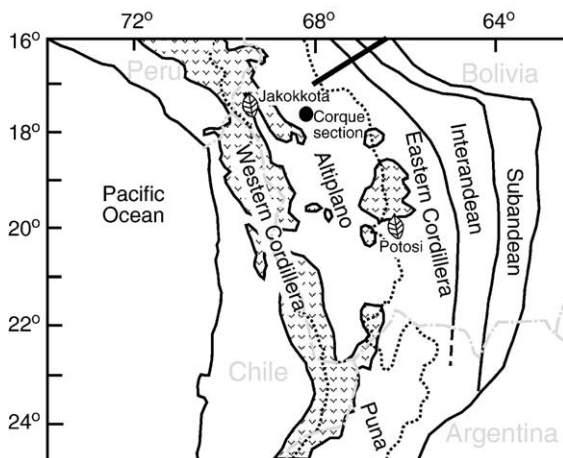


Fig. 1. Topographic and tectonic provinces of the central Andes. The dotted lines mark the crests of the Eastern and Western Cordilleras, which define the limits of internal drainage within the Altiplano [16,74]. The dashed gray lines are political boundaries. The black circle is our carbonate sampling locality and leaf symbols indicate paleoleaf localities [26,27]. The thick black line is the approximate location of the rainfall transect [1].

of eclogitic lower crust below the Andean plateau. Crustal thickness variations in the central Andes from broadband recordings of P-to-S wave conversions at the Moho (receiver functions) indicate that the topography of the Andean plateau reflects Airy isostatic conditions, with crustal thicknesses in excess of 70 km below the Eastern and Western Cordillera and between 59 and 64 km in the central Altiplano [28,29]. Seismic tomography of the mantle between 16° and 20°S shows low P-wave speeds below the Altiplano–Eastern Cordillera transition and relatively high P-wave speeds below the central Altiplano and Subandean zone [30,31]. These studies suggest that virtually all of the mantle lithosphere below the eastern Altiplano and western part of the Eastern Cordillera has been removed, which is consistent with high $^3\text{He}/^4\text{He}$ ratios across much of the Altiplano and Eastern Cordillera, interpreted to reflect degassing of mantle-derived magmas [32]. Although the crustal column below the Western Cordillera magmatic arc shows typical high-speed lower crust, the crustal column below the Altiplano shows no high-speed lower crust and appears to consist of felsic composition similar to that of upper crust [29]. These observations have been used to support previous suggestions [4,6] that not only the mantle lithosphere, but also eclogitic lower crust below the Altiplano and western part of the Eastern Cordillera has been removed [29]. The eruption of mafic lavas throughout the northern and central Altiplano beginning at ~7.5 to 5.5 Ma concurs with thinning or removal of mantle lithosphere by this time [18,33], whereas mafic volcanic rock of ≤ 3 Ma in the southern Altiplano and Puna has been inferred to reflect Pliocene removal of eclogitic lower crust and mantle lithosphere beneath the Puna plateau [6,34].

3. Modern climate and historical atmospheric circulation

Oxygen isotope paleoaltimetry is most applicable in regions that experience a moderate amount of rainfall (>0.5 m/yr) and where long-term patterns of atmospheric circulation are understood. The orientation of the Andean orogenic belt displays a large bend at ~18°S that marks the approximate location of significant changes in rainfall amount and atmospheric circulation. North of the bend in the Andes, the Altiplano receives between ~0.6 and 1.2 m/yr of rainfall, whereas south of the bend, rainfall rarely exceeds ~0.5 m/yr [35–37]. Most of the rainfall in the northern Altiplano occurs during the austral summer and is derived from the Amazon basin. The Altiplano north of the bend is

ideal for oxygen isotope paleoaltimetry because the higher rate of rainfall minimizes evaporative enrichment of ^{18}O in rain and surface waters, which can lead to an underestimation of paleoelevation.

Historical changes in the source of moisture can influence the isotopic composition of high elevation precipitation, because different vapor transport pathways affect both the composition of source moisture and the degree of fractionation of a vapor mass [38]. It is therefore important to understand long-term changes in climate and their implications for changes in atmospheric circulation. Several studies suggest that extremely arid conditions in the western Andes and forearc were established between ~10 and 14 Ma, consistent with a long term source of moisture from the Amazon with a significant orographic barrier [39,40]. In addition, long term patterns of high erosional denudation north of the bend in the Andes versus low erosional denudation south of the bend suggest that modern latitudinal patterns of atmospheric circulation characterized the past 10 to 15 Myr [41].

4. Stratigraphy

4.1. Age constraints

We measured and sampled stratigraphic sections in the eastern limb of the Corque syncline near Callapa (Fig. 2A). Today these deposits sit at elevations between ~3800 and 3900 m. Magnetic polarity stratigraphy [42], with ties to the geomagnetic polarity time scale from $^{40}\text{Ar}/^{39}\text{Ar}$ dates of volcanic rock within the section [43], constrains the age of pre-9 Ma rock in the sections. Our magnetostratigraphy (Fig. 2B) provides age constraints between the Callapa tuff (9.03 ± 0.07 Ma) and Toba 76 tuff (5.348 ± 0.003 Ma) [43].

Samples from 1200 m of red sedimentary rock exposed between or just above the Callapa and Toba 76 tuffs were used for magnetostratigraphic analysis. We took 3–4 hand samples from each of 56 sites using standard techniques [45]. Most samples were demagnetized via thermal demagnetization; alternating field demagnetization of samples from two sites was unsuccessful. Typical unblocking temperatures for characteristic remanent magnetization are between 600 and 660 °C, suggesting that hematite is the dominant mineral carrying the characteristic remanence. For 108 samples we obtained line fits on the thermal demagnetization steps with maximum angular deviation <15°, and all other samples were rejected from further analysis. Magnetostratigraphy is based upon virtual geomagnetic polarity (VGP) results from 43 sites,

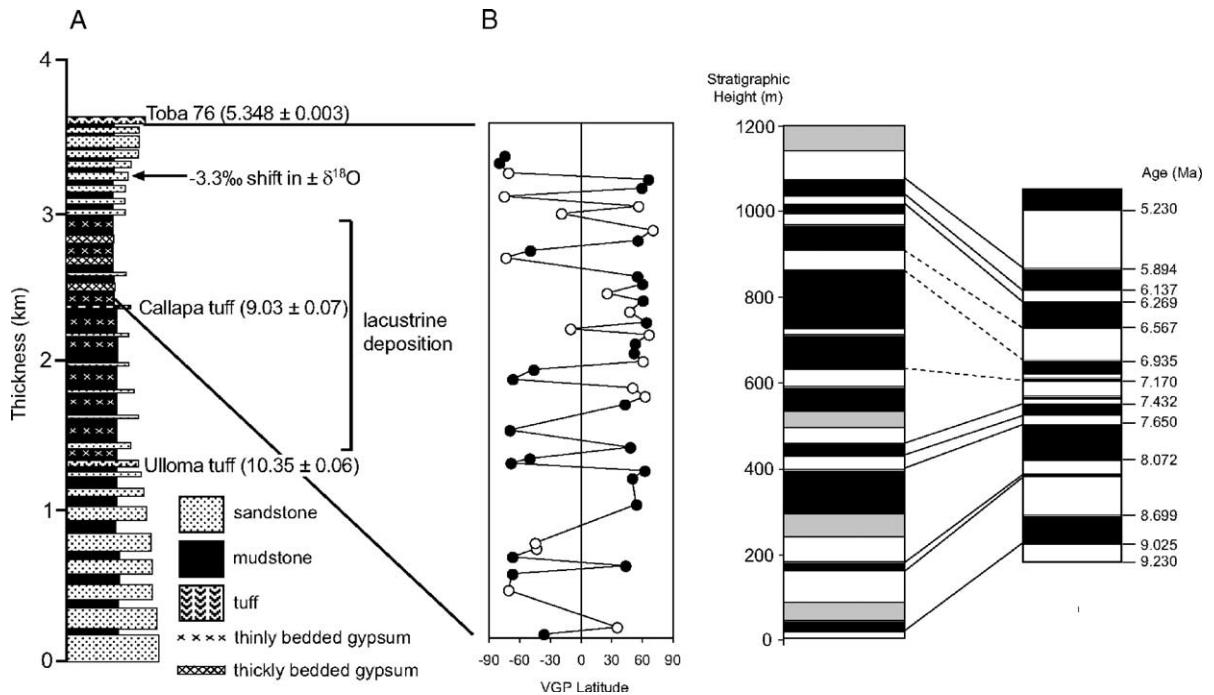


Fig. 2. Stratigraphy and magnetostratigraphic correlation. A. Schematic representation of measured stratigraphic sections in the eastern limb of the Corque syncline, near Callapa. Stratigraphic level of dated tuffs [43] and the isotopic shift within the section are shown. B. Correlation of magnetic polarity stratigraphy to geomagnetic polarity time scale [75]. Site-means of virtual geomagnetic pole (VGP) plotted versus stratigraphic level above the Callapa tuff. Positive latitude indicates normal polarity shown as black intervals; negative latitude indicates reversed polarity shown as white intervals. Filled circles are class A sites (2 or more samples with good demagnetization) and open circles are class B sites (1 sample with good demagnetization).

with reversals tied directly to the stratigraphic section (Fig. 2).

4.2. Depositional environments

Although we rely on $\delta^{18}\text{O}$ of carbonate to quantify elevation, the sedimentary record contains additional paleoenvironmental information that can help us evaluate how faithfully the isotopes record paleoelevation. Multistory lenticular sand bodies up to 15 m thick and massive to laminated red-brown mudstones at the base of the section represent fluvial and floodplain facies. We interpret the predominantly mudstone interval between the Ulloma tuff (10.35 ± 0.06 Ma) and that dated at ~ 7.6 Ma to be lacustrine (Fig. 2A). This mudstone unit can be traced laterally for tens of kilometers, as far as we could follow it, suggesting a widespread lake system. Fluvial and floodplain deposition resumed in the upper 700 m of the section, which displays coarsening upward and consists of lenticular sand bodies up to 5 m thick, alternating with massive to laminated mudstones. We use these interpretations of depositional environment to evaluate

the subenvironments of carbonate deposition to determine the fidelity of oxygen isotope paleoelevation estimates.

Fluvial-floodplain and lacustrine intervals contain authigenic carbonates that we sampled for O and C isotopes (Table 1). The floodplain lithofacies contain both paleosol carbonate nodules and palustrine carbonates. Paleosols are massive and red to reddish brown, with red color decreasing with depth in the paleosol, which we interpret as reflecting decreased oxidation with depth. Discrete carbonate (Bk) horizons, including rare carbonate rhyoliths, occur below the upper part of the B horizon that has been leached of carbonate. We sampled micritic paleosol carbonate nodules in all cases between ~ 20 and 80 cm below the top of the paleosol. Nodules are 0.5 to 3 cm in diameter and display rare root tubules. Palustrine carbonates represent marsh or shallow pond deposits in the floodplain adjacent to fluvial channels. We presume that these laminated, mud-rich micrites precipitated seasonally when evaporation rates and productivity were higher. Rare carbonates deposited in the lacustrine interval include laminated, very thinly bedded, micritic limestone that

Table 1
Oxygen and carbon isotope data from stratigraphic sections sampled in the eastern limb of the Corque syncline

Sample name	Description	Stratigraphic level	Age	$\delta^{18}\text{O}(\text{VPDB})$ (‰)	$\delta^{13}\text{C}(\text{VPDB})$ (‰)
Section 1—below Ulloma tuff					
Bottom of section: S17° 34' 49.7" W68° 16' 28.6"					
Top of section: S17° 34' 19.4" W68° 17' 47.2"					
03BL4	Sandstone cement	27	11.54	−12.5	−8.1
*				−12.6	−8.2
03BL5	Palustrine carbonate	61	11.51	−9.7	−8.2
*				−9.5	−8.6
03BL7	Palustrine carbonate	76	11.49	−9.6	−6.4
03BL9	Paleosol carbonate nodule	120	11.45	−13.3	−8.3
03BL12	Paleosol carbonate nodule	134	11.43	−11.3	−9.2
03BL13	Paleosol carbonate nodule	143	11.42	−11.4	−9.5
*				−11.3	−9.4
03BL15	Palustrine carbonate	185	11.38	−12.9	−9.1
03BL16	Palustrine carbonate	192	11.37	−9.7	−8.8
03BL18	Palustrine carbonate	201	11.36	−13.3	−7.4
03BL19	Paleosol carbonate nodule	243	11.32	−11.8	−7.2
03BL20	Palustrine carbonate	263	11.30	−10.6	−8.5
*				−10.6	−8.5
03BL21	Palustrine carbonate	265	11.29	−10.2	−8.3
03BL23	Palustrine carbonate	334	11.22	−9.9	−8.7
03BL25	Paleosol carbonate nodule	407	11.15	−12.7	−8.1
03BL26	Palustrine carbonate	425	11.13	−12.0	−8.4
03BL28	Paleosol Carbonate nodule	471	11.08	−11.9	−11.4
*				−11.9	−11.6
04BL69	Paleosol carbonate nodule	594	10.95	−9.5	−10.3
04BL72	Reworked rhyolith	646	10.90	−12.5	−8.46
04BL75	Paleosol carbonate nodule	667	10.88	−12.5	−8.5
04BL76	Paleosol carbonate nodule	801	10.74	−12.0	−8.4
04BL77	Paleosol carbonate nodule	940	10.59	−11.1	−8.7
04BL78	Paleosol carbonate nodule	955	10.58	−12.7	−9.4
04BL79	Paleosol carbonate nodule	1004	10.53	−10.9	−9.4
04BL80	Paleosol carbonate nodule	1067	10.46	−10.5	−10.2
03BL1	Paleosol carbonate nodule	1189	10.33	−12.6	−8.3
*				−12.7	−8.3
Section 2—between Ulloma tuff and Callapa tuff					
Bottom of section: S17° 23' 35.8" W68° 24' 4.1"					
Top of section: S17° 24' 19.5" W68° 24' 34.0"					
03BL29	Lacustrine calcareous mudstone	18	10.10	−9.0	−8.9
03BL31	Lacustrine calcareous mudstone	56	10.05	−10.3	−9.0
03BL32	Lacustrine micrite	88	10.015	−9.8	−12.5
03BL33	Lacustrine micrite	90	10.013	−10.2	−5.3
03BL34	Lacustrine micrite	90	10.013	−9.6	−6.2
03BL35	Lacustrine micrite	125	9.97	−9.0	−3.6
03BL36	Lacustrine micrite	147	9.95	−8.5	−11.7
03BL37	Sandstone cement	157	9.94	−10.6	−11.4
03BL39	Lacustrine calcareous mudstone	259	9.82	−9.4	−12.0
03BL40	Lacustrine calcareous mudstone	271	9.81	−11.6	−10.4
*				−11.5	−10.5
03BL41	Lacustrine calcareous mudstone	277	9.80	−9.4	−15.6
04BL36	Lacustrine calcareous mudstone	440	9.61	−8.1	−9.38
04BL38	Lacustrine calcareous mudstone	470	9.58	−9.9	−11.8
04BL42	Lacustrine calcareous mudstone	506	9.54	−5.6	−11.6
04BL46	Lacustrine calcareous mudstone	571	9.46	−9.7	−6.5
04BL48	Lacustrine calcareous mudstone	597	9.43	−9.8	−6.6
04BL54	Lacustrine calcareous mudstone	689	9.33	−8.0	−11.2
04BL55	Lacustrine calcareous mudstone	725	9.29	−8.7	−7.5
04BL58	Lacustrine calcareous mudstone	785	9.22	−9.1	−7.7

(continued on next page)

Table 1 (continued)

Sample name	Description	Stratigraphic level	Age	$\delta^{18}\text{O}(\text{VPDB}) (\text{‰})$	$\delta^{13}\text{C}(\text{VPDB}) (\text{‰})$
04BL59	Lacustrine calcareous mudstone	811	9.19	−7.5	−8.1
04BL62	Lacustrine micrite	866	9.12	−7.8	−4.8
04BL64	Lacustrine micrite	889	9.10	−7.5	−3.6
Section 3—between Callapa tuff and Toba 76					
Bottom of section: S17° 37' 09.9" W68° 17' 49.1"					
Top of section: S17° 37' 46.3" W68° 18' 33.9"					
03BL43	Lacustrine calcareous mudstone	154	8.58	−9.3	−8.4
03BL44	Lacustrine calcareous mudstone	168	8.54	−9.1	−9.3
04BL1	Sandstone cement	303	8.11	−10.1	−9.7
04BL2	Paleosol carbonate nodule	413	7.61	−12.8	−2.8
04BL6	Palustrine carbonate	521	7.39	−10.5	−6.9
04BL4	Palustrine carbonate	532	7.38	−11.3	−10.8
04BL5	Palustrine carbonate	545	7.37	−10.9	−12.1
04BL7	Palustrine carbonate	573	7.353	−10.6	−9.3
04BL8A	Palustrine carbonate	575	7.352	−14.1	−7.8
*				−14.1	−7.9
04BL8B	Palustrine carbonate	575	7.352	−10.6	−7.8
04BL8C	Palustrine carbonate	575	7.352	−14.0	−7.8
04BL9	Palustrine carbonate	579	7.349	−12.9	−6.8
04BL10	Paleosol carbonate nodule	600	7.32	−12.8	−5.8
04BL11	Palustrine carbonate	627	7.24	−11.5	−6.9
04BL12	Palustrine carbonate	631	7.23	−10.0	−8.3
04BL14	Palustrine carbonate	752	6.94	−12.4	−7.4
04BL15A	Palustrine carbonate	762	6.92	−9.2	−8.8
04BL15B	Palustrine carbonate	762	6.92	−8.3	−8.8
04BL15C	Palustrine carbonate	762	6.92	−8.7	−8.8
04BL16	Palustrine carbonate	786	6.86	−10.4	−8.0
04BL17	Palustrine carbonate	794	6.84	−12.4	−8.2
04BL19	Sandstone cement	815	6.79	−15.1	−9.1
04BL21	Paleosol carbonate	839	6.74	−15.3	−6.9
04BL23	Sandstone cement	858	6.69	−14.0	−9.2
04BL24	Paleosol carbonate	883	6.64	−13.8	−6.3
04BL25	Paleosol carbonate	925	6.53	−14.4	−4.6
04BL26	Sandstone cement	950	6.46	−14.8	−7.2
04BL27	Sandstone cement	953	6.45	−15.1	−7.6
04BL28	Sandstone cement	985	6.36	−14.8	−10.0
04BL30	Paleosol carbonate	1080	5.83	−15.1	−6.6
04BL31	Paleosol carbonate	1112	5.46	−9.6	−3.7

Errors on $\delta^{18}\text{O} = \pm 0.1$ and $\delta^{13}\text{C} = \pm 0.06\text{‰}$ based on repeated standard measurements. VPDB—Vienna Pee Dee belemnite. * Represents replicate analyses of the same powder. Samples labeled A, B, and C represent replicate analyses of separate powders from the same sample locality. Ages in sections 1 and 2 were extrapolated from on $^{40}\text{Ar}/^{39}\text{Ar}$ tuff ages (32) and magnetostratigraphy (31). Ages in Section 3 were extrapolated from magnetostratigraphy in this study.

contains vertical worm burrows and laminated, thinly to thickly bedded, calcareous mudstones. Inspection of thin sections reveals that paleosol, palustrine, and lacustrine carbonates lack sparry calcite, suggesting that they have not undergone extensive, late-stage diagenesis. This inference is supported by paleothermometry data that indicate that the carbonates precipitated at temperatures representative of modern surface temperatures in the central Andes [44] rather than at higher temperatures that reflect the depth of burial. Carbonate cements were sampled in fluvial channel deposits. Here we report results only from micritic cements interpreted to have been deposited in the vadose zone [46].

5. Oxygen isotope paleoaltimetry

Topography affects the degree of rainout (water condensation of a vapor mass), because adiabatic decompression of an ascending air mass causes cooling and condensation. Partitioning of ^{18}O and ^2H into the liquid phase, as rainout proceeds, leads to a progressive decrease in $\delta^{18}\text{O}$ and $\delta^2\text{H}$ values of both the vapor mass and rain derived from it [1,47–50]. Samples of surface water or rainfall across a topographic gradient yield a local, empirical relationship between $\delta^{18}\text{O}$ and altitude [1,48] that then can be used to infer paleoelevations. Oxygen isotopic composition of lacustrine and paleosol

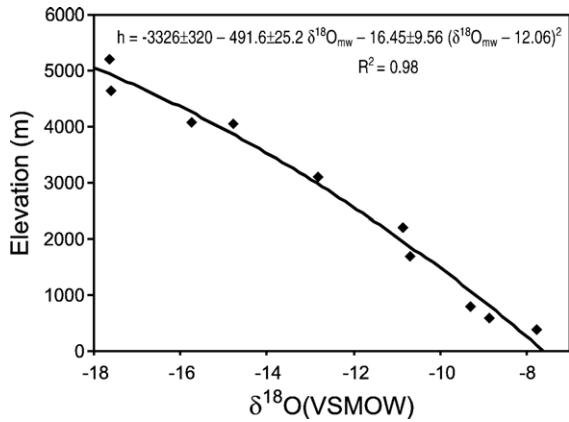


Fig. 3. $\delta^{18}\text{O}$ (relative to Vienna standard mean ocean water, VSMOW) of rainfall in 1984 [1]. The solid black line is the 2nd order polynomial fit used to calculate paleoelevation.

carbonates depend on paleoelevation because they are determined largely by the $\delta^{18}\text{O}$ value of the meteoric water ($\delta^{18}\text{O}_{\text{mw}}$) from which they precipitated [51–53]. By assuming a temperature of carbonate precipitation and applying a temperature-dependent fractionation equation [54], we may calculate the $\delta^{18}\text{O}$ value of paleo-meteoric water from the $\delta^{18}\text{O}$ of surface carbonates ($\delta^{18}\text{O}_{\text{c}}$) and compare it to the local $\delta^{18}\text{O}_{\text{mw}}$ vs. altitude relationship to determine paleoelevation [48].

Rainfall sampled in 1984 at 10 stations over an elevation transect adjacent to the northern Altiplano displays a systematic decrease in weighted mean annual $\delta^{18}\text{O}$ values from -7.8‰ at 395 m to -17.6‰ at 5200 m [1]. Although 2 years of data (1983 and 1984) are reported, we used only rainfall data for 1984 (Fig. 3A) to determine the local relationship of $\delta^{18}\text{O}_{\text{mw}}$ to altitude (Fig. 3):

$$h = -3326 \pm 320 - 491.6 \pm 25.2 \delta^{18}\text{O}_{\text{mw}} - 16.45 \pm 9.56 (\delta^{18}\text{O}_{\text{mw}} - 12.06)^2 \quad (1)$$

where h is elevation in km and the $R^2=0.98$, because this reflects a typical year for rainfall amount. The summer rainy season of 1983 was affected by drought, producing relatively positive $\delta^{18}\text{O}$ values compared to a typical year [1].

6. Methods and materials

We analyzed paleosol, palustrine, and lacustrine carbonates and sandstone cements for their O and C isotopic compositions (Fig. 4, Table 1). Samples showing any evidence of sparite were micromilled using a 20 μm drill bit to avoid diagenetic phases. Carbonates were analyzed

at the University of Arizona using an automated carbonate preparation device (Kiel-III) coupled to a Finnigan MAT 252.

To calculate the uncertainty on paleoelevation estimates, we exploited 1000 Monte Carlo simulations of the relationship between $\delta^{18}\text{O}$ and altitude given by Eq. (1) and shown in Fig. 3A. These simulations took into account not only (1) the scatter in the empirical $\delta^{18}\text{O}$ vs. altitude relationship, but also (2) uncertainties in the empirical temperature-dependent fractionation equation, $1000 \ln_{\text{c-w}} \alpha = 18.03 \pm 0.36 (1000T^{-1}) - 32.42 \pm 1.22$ [54], and (3) uncertainty in the assumed temperature of carbonate precipitation of $\pm 5^\circ\text{C}$. Monte Carlo simulation is preferable to geometric estimation in the case of significant covariance, and covariance is most specifically observed here between $\delta^{18}\text{O}$ vs. elevation fit coefficients and temperature of carbonate precipitation.

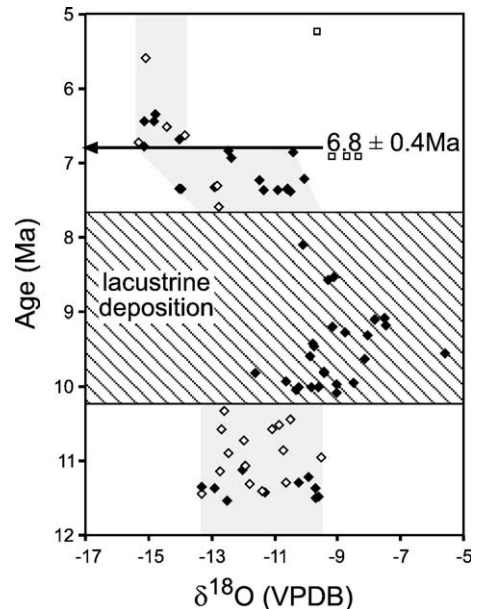


Fig. 4. $\delta^{18}\text{O}$ (relative to Vienna Peedee belemnite, VPDB) of carbonates versus stratigraphic level for section shown in Fig. 2A. Ages are constrained by $^{40}\text{Ar}/^{39}\text{Ar}$ dates on tuffs [43], previously published magnetostratigraphy [42], and our magnetostratigraphy (Fig. 2B). Open diamonds are paleosol carbonates, and all other symbols are lacustrine and palustrine carbonates. Relatively positive $\delta^{18}\text{O}$ values during the time period represented by lacustrine deposition probably reflect increased evaporative enrichment of ^{18}O . Gray bands show the range of $\delta^{18}\text{O}$ values used in the paleoelevation analysis, excluding the lacustrine interval. Two outliers, including one sample with three replicate analyses, (open squares) were excluded from the paleoelevation analysis shown in Fig. 5. A 3‰ to 4‰ shift to more negative $\delta^{18}\text{O}$ values occurs between 10.3 Ma and 6.8 ± 0.4 Ma (Table 1). We choose a conservative uncertainty of ± 0.4 Ma on the minimum age constraint on the timing of the isotopic shift assuming that the magnetostratigraphy failed to record one normal polarity interval and the correlation could be shifted by one reversed polarity chron.

Monte Carlo estimation yields 1σ errors in oxygen isotope paleoelevations that decrease from ± 1000 m at the lowest paleoelevations to ± 500 m at highest paleoelevations.

7. Results and discussion

7.1. Paleoelevation estimates

Carbonates in the lacustrine interval between 10.3 and 8 Ma display a wide range of isotopic compositions with relatively positive $\delta^{18}\text{O}_c$ values between -11.6‰ and -5.6‰ (Fig. 4). Less negative values during this time period probably reflect evaporative enrichment of ^{18}O in lake water associated with closed basin conditions. This inference is supported by Holocene closed basin lakes in the northern Altiplano that have inferred $\delta^{18}\text{O}$ values of lake water between -17‰ and -4‰ [55], approaching much less negative $\delta^{18}\text{O}$ values than meteoric water at the same elevation (Fig. 3). Because ^{18}O enrichment leads to an underestimate of elevation, we exclude these data from the paleoelevation analysis. From 11.5 to 10.3 Ma, all carbonates fall between -9.5‰ and -13.3‰ . Between 7.6 and 6.8 Ma, carbonates range between -14.1‰ and -8.3‰ , displaying a wider range of values than both prior to 10.3 Ma and after 6.8 Ma. By 6.8 ± 0.4 Ma, there is a 3‰ to 4‰ shift in the mean $\delta^{18}\text{O}_c$ to values that range between -13.8‰ and -15.3‰ , except for one relatively posi-

tive outlier ($\delta^{18}\text{O}_c = -9.6\text{‰}$). Qualitative assessment of these data, compared with late Miocene paleoelevation estimates of no more than 1.6 km from leaf physiognomy [27], suggests that the Altiplano had attained its current elevation by 6.8 Ma and rose some time between 10.3 and 6.8 Ma.

One of the largest sources of error in carbonate oxygen isotope paleoaltimetry stems from uncertainty in the temperature of carbonate precipitation. Empirically derived temperature dependence shows a change in $\delta^{18}\text{O}_c$ values of $\sim 0.21\text{‰}/^\circ\text{C}$ [54]. To mitigate this uncertainty we used temperature estimates from a new paleothermometry technique [56] applied to paleosol carbonates within our section [44]. A high average temperature of 28.4°C was obtained from paleosols older than 10.3 Ma. An intermediate average temperature of 17.7°C reflects 2 paleosols deposited between 7.6 and 7.3 Ma. Paleosols younger than 6.8 Ma record a low average paleotemperature of 12.6°C , which is similar to modern warm season temperatures in this region of 12°C (average monthly temperature for the warmest month of the year, data from the Global Historical Climatology Network; El Alto, 16.50°S 68.20°W , elev=4103 m, November). For the time period between 10.3 and 6.8 Ma, we assumed that temperature decreased linearly from 28.4 to 12.6°C .

We used the northern Altiplano $\delta^{18}\text{O}_{\text{mw}}$ vs. altitude relationship (1) to estimate paleoelevation from the $\delta^{18}\text{O}$ of paleo-meteoric water (Fig. 5). Between 11.5

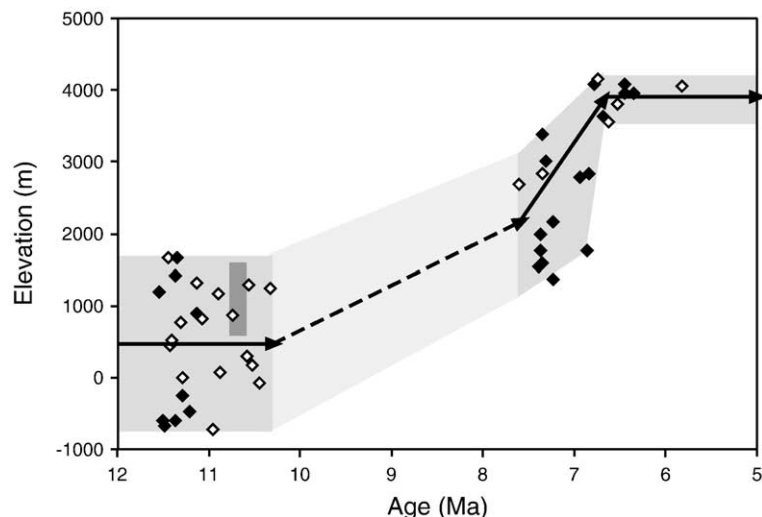


Fig. 5. Compilation of paleoelevation estimates from oxygen isotopes in carbonates (medium gray) and paleoleaf physiognomy (dark gray bar). Open diamonds are estimates from paleosol carbonates, and closed diamonds are palustrine carbonates. Paleoelevation estimates from both fossil leaves and carbonates prior to ~ 10.3 Ma overlap in range and indicate that no more than one half of the modern elevation was obtained. Paleoelevation constraints are lacking between 10.3 Ma and 7.6 Ma (light gray), during the time period of widespread lacustrine deposition within our section. Based on O isotopes, uplift of ~ 2.5 to 3.5 km occurred between ~ 10.3 and 6.8 ± 0.4 Ma isotopes, followed by similar to modern elevations in the Altiplano.

Ma and 10.3 Ma, paleoelevations were between -700 ± 1000 m and 1700 ± 700 m. Intermediate paleoelevations of 1400 ± 700 m to 3400 ± 500 m were calculated between 7.6 and 6.8 Ma. By 6.8 Ma, consistently high elevations of 3500 ± 500 m to 4200 ± 500 m were estimated. These paleoelevation estimates and our magnetostratigraphy suggest that surface uplift of the Altiplano on the order of 2.5 to 3.5 km occurred over a ~ 1 to 4 Myr time period between 10.3 and 6.8 Ma.

Negative elevations calculated for the oldest time period are probably a reflection of evaporative enrichment of ^{18}O in surface water. Palustrine carbonates make up all but one of the samples that yielded a negative elevation (Fig. 5). These carbonates, deposited in shallow pond or marsh settings within fluvial floodplain environments, most likely experienced enhanced precipitation during seasonal dry periods when evaporation rates were highest. The observation that paleosol carbonates generally yield higher elevation estimates suggests that they reflect less evaporative enrichment of ^{18}O and provide a better proxy for elevation.

7.2. Implications for lithospheric processes

Crustal shortening within the central Bolivian Andes can account for crustal thickness in the northern Altiplano [16,57,58]. Although the crustal thickness beneath the Altiplano exceeds that nearly everywhere on earth, rapid crustal thickening beneath this region offers an unlikely mechanism to account for the rapid increase in elevation. Where crustal shortening leads to crustal thickening, the product of the shortening rate, u , and crustal thickness, H , should equal the product of the width of the deforming region, W , and the average rate of crustal thickening, dH/dt : $u H = W dH/dt$. Insofar as Airy isostasy is approximately maintained during shortening, the surface should rise at a rate, dh/dt , given by:

$$\frac{dh}{dt} = \frac{(\rho_m - \rho_c)}{\rho_c} \frac{dH}{dt} = \frac{(\rho_m - \rho_c)}{\rho_c} \frac{uH}{W} \approx \frac{1}{5.5} \frac{uH}{W} \quad (2)$$

where $\rho_c (= 2.8 \times 10^3 \text{ kg/m}^3)$ and $\rho_m (= 3.3 \times 10^3 \text{ kg/m}^3)$ are the densities of crust and mantle, Using a maximum long term shortening rate over the past 10 Myr of $u = 10$ mm/yr [21] over a plateau width of $W = 300$ km and an initial crustal thickness of $H = 50$ km, the average rate of elevation change, dh/dt , should be $\sim 3\%$ of the crustal shortening rate, u , or 0.3 mm/yr. Correspondingly, to achieve 1 km of elevation gain requires 3–4 Myr, and 3 km requires 10 Myr. As-

suming crustal shortening occurred between 10.7 Ma, the only time for which paleoelevation estimates from both fossil leaves and oxygen isotopes exist, and 6.8 Ma, the initial timing of paleoelevations consistent with modern, then crustal thickening of 8 km over ~ 4 Myr could raise the surface ~ 1.2 km. This estimate ignores both the countering effect of shortening and thickening the mantle lithosphere and the width of the Eastern Cordillera, which also seems to have risen since 10 Ma [19,24], but it is still insufficient to generate the minimum amount of surface uplift indicated by the oxygen isotope data.

Having eliminated crustal thickening as a means of changing the density structure of the lithosphere over the requisite timescale, the only plausible remaining process is to alter the density structure of the mantle, either by a change in temperature or composition. Because diffusion of heat is slow, only removal of mantle lithosphere seems capable of inducing surface uplift in excess of 2.5 km in a period as short as a few million years. Crust and mantle lithosphere might delaminate by mantle lithosphere peeling away from crust and sinking into the asthenosphere [2], or convective instability might grow rapidly by blobs of mantle lithosphere sinking into the asthenosphere, as material in adjacent regions feeds the blob and thins [59]. In either case, the replacement of relatively dense mantle lithosphere with hotter, lighter asthenosphere reduces the load beneath the plateau, and because of isostasy, the surface should rise.

A 2.5 to 3.5 km rise of the Altiplano in a period as short 1 to 4 Myr implies an average vertical speed between 3.5 and 0.6 mm/yr. These rates are approximately an order of magnitude lower than those for post-glacial rebound of Canada and Fennoscandia [60,61], where rapid vertical movement occurs over a much larger area than the Altiplano. Viscous flow in the asthenosphere dictates the rate of rebound, and the upper bound on the viscosity beneath the Altiplano [62] is smaller than that beneath the Canadian and Fennoscandian shields [60]. Thus, viscous resistance to vertical movement of the Altiplano seems unlikely to have prevented the inferred vertical movement and average speed.

Several other studies provide indirect evidence that support the timing, magnitude of elevation change, and removal of eclogitic lower crust and mantle lithosphere as the mechanism triggering the abrupt rise of the Andean plateau. Data from the 10.66 ± 0.06 Ma Jakokkota flora [27] overlap our estimates for the early late Miocene (Fig. 5). The widespread ~ 1.5 to 2 km incision of the paleosurfaces in the Eastern Cordillera, begin-

ning by ~ 6.5 Ma [24], agrees with both the timing and magnitude of uplift that we observe. Recent thermochronology in the Eastern Cordillera suggests an onset of rapid incision between ~ 7 and 5 Ma despite lack of evidence of upper crustal shortening [63], consistent with the timing that we infer. The eruption of mafic lavas throughout the northern and central Altiplano beginning at ~ 7.5 to 5.5 Ma [18,33] reflects a minimum age for the removal of mantle lithosphere, consistent with the onset of surface uplift between 10.3 and 7.6 Ma suggested by paleoelevation estimates (Fig. 5).

A late Miocene change in the style of deformation in the Altiplano provides further support for removal of mantle lithosphere. Widespread contractional deformation took place across the Altiplano basin between ~ 25 and 7 Ma, accounting for ~ 30 km of shortening [18], while the Interandean zone (transition between Eastern Cordillera and Subandes) accommodated most of the shortening in the Andean fold-thrust belt [16,17]. Most shortening within the Altiplano ceased by ~ 7 Ma [64], accompanied by the formation of a regional unconformity between ~ 7 and 5 Ma and a significant decrease in sedimentation rate [18,65]. Removal of mantle lithosphere and isostatic rebound of the Andean plateau should elevate the surface, which in turn should increase the vertical compressive stress at all levels beneath the plateau. Accordingly, the horizontal *deviatoric* compressive stress across the plateau should have decreased [10], in agreement with the decrease in the rate of shortening and initiation of regional neplanation at ~ 7 Ma.

7.3. Fold-thrust belt evolution and plate motions

Insofar as fold-thrust belts behave as wedge-shaped bodies of rock whose constitutive law is governed by Coulomb friction, they maintain a “critical taper” where the net (horizontal) force per unit length driving the wedge forward is balanced by basal friction resisting advance of the wedge [66,67]. The wedge geometry or “taper” is described by the sum of the décollement slope (β) and the surface slope (α). Changes in the force per unit length applied to the rear of the wedge, in either pore pressure or the coefficient of friction within the wedge, and in the basal shear stress can alter the taper of the wedge: $\alpha + \beta$. If a change in any of these variables causes the wedge to become “supercritical” ($\alpha + \beta >$ critical taper), then the taper will decrease by lengthening, either through forward propagation of deformation at the front of the wedge [68] or normal faulting and horizontal extension within the wedge. Alternatively, a fold-thrust belt wedge can become supercritical without a change in the taper by rotation of

the wedge such that α increases while β decreases (i.e., subsidence of the front of the wedge or uplift of the rear of the wedge). The rise of the Andean plateau by removal of mantle lithosphere can transform the state of the Andean fold-thrust belt from critical to supercritical, because of either 1) the increase in the horizontal force per unit length acting on the wedge or 2) the decrease in β and increase in α associated with elevating the rear of the fold-thrust belt wedge. The eastward propagation of deformation into the Subandean zone in late Miocene time [19–21] may be another manifestation of the rapid rise of the Andean plateau. The most precise dating indicates 7.6 Ma for the timing of the eastward jump in deformation [21], consistent with the minimum timing of inferred rapid rise of the northern Altiplano.

Not only did the locus of deformation within the Andes shift between 8 and 7 Ma, but also the rate of convergence between the Nazca and South America plates dropped by approximately 30% between ~ 8 and 5 Ma (Fig. 6). Cande et al. [69] showed that the rate of opening between the South America and Africa plates slowed since 10 Ma, and Tebbens and Cande [70] report a similar decrease in speed between the Nazca and Antarctica plates. To calculate relative positions of the Nazca and South America plates at different times, we combined plate reconstructions for the sequence South America \rightarrow Africa \rightarrow Antarctica \rightarrow Nazca for times since 12 Ma, and for the earlier period, we reconstructed the sequence South America \rightarrow Africa \rightarrow Antarctica \rightarrow Pacific \rightarrow Nazca (Fig. 6). Despite uncertainties in reconstructions, a change in rate must have begun since ~ 8 Ma and was largely completed by 5 Ma (Fig. 6). If it occurred abruptly, the change occurred between 5 and 6 Ma. In either case, most of the change occurred after the Altiplano rose to its present elevation.

Removal of mantle lithosphere below the Andean plateau increases the force per unit length that the plateau applies to the surrounding lowlands [10,71]. The increase in force per unit length ΔF_L depends on the density of crust ρ_c , the change in mean elevation, Δh , the crustal thickness H , and the thickness of the layer of mantle lithosphere L that is removed (Fig. 7):

$$\Delta F_L \approx \rho_c g \Delta h \left(\frac{\Delta h}{2} + H + \frac{L}{2} \right). \quad (3)$$

Inserting appropriate numbers, such as $\Delta h = 2$ km, $H = 60$ km, and $L = 100$ km, yields 6×10^{12} N/m, nearly twice that of “ridge push” [72,73]. If the entire Andean belt, not just the Altiplano and adjacent area, had risen 2000 m because of removal of mantle lithosphere, we might expect convergence between the Nazca and

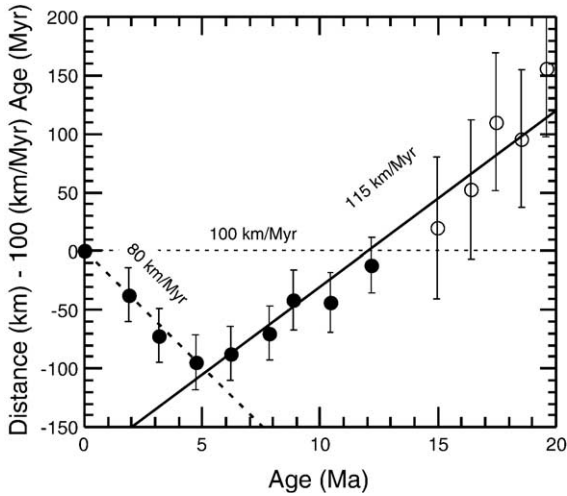


Fig. 6. Reconstructed distances of a point presently at 20°S, 70°W on the South America plate to the Nazca plate. To show the change in rate clearly, distances are reduced by subtracting the product of a rough average rate of 100 km/Myr times the age from each distance. Dotted, dashed, and solid lines show rates of 100, 80, and 115 km/Myr. Least-squares fits to distances for 8–20 Ma and for 0–5 Ma are 117 ± 4 and 79 ± 13 km/Myr, respectively. For all reconstructions, we used those of Cande et al. [69] for the South Atlantic (South America to Africa). To reconstruct Africa to Antarctica, we relied on studies focused on different precise times [76–78], and we interpolated between them to obtain parameters for the same times used by Cande et al. [69]. Then to reconstruct Antarctica to the Nazca plate, we interpolated between reconstructions of these plates given by Tebbens and Cande [70] for times since 12 Ma. For earlier periods, we reconstructed Antarctica to the Pacific plate interpolating between Cande and Stock’s [79] parameters, and then Pacific to Nazca using interpolations of parameters given by Cande and Kent [80] for ~10 Ma and Pardo-Casas and Molnar [81] for ~21 Ma. In all cases, we relied on uncertainties given by the various authors. Uncertainties are smaller for times of reconstructions since 12 Ma (closed circles) than for the earlier period (open circles) for two reasons: first, at each time between 20 and 12 Ma, we combined four instead of three reconstructions, and second, parameters for Pacific–Nazca reconstructions are much less accurate than those of other plate pairs.

South America plates to stop altogether, or at least a greater change in relative movement to have occurred than the 30% decrease in rates between 5 and 8 Ma (Fig. 5). Nevertheless, if a segment of the Andes only 500 km in length, roughly 10% of the length of the Nazca–South America plate boundary, rose 2000 m, the average increase in the force per unit length of 0.6×10^{12} N/m would still be ~20% of “ridge push.” The ~30% change in the convergence rate, therefore, implies that the forces that drive plates are delicately balanced, and that changes in those forces equal to a fraction of any of the major forces can alter the rate of relative plate motion. Perhaps more important here, its occurrence corroborates the inference that lower crust and mantle lithosphere were removed.

Because the rise of the Altiplano occurred before the change in rate was completed, we cannot infer that the change in rate caused the increase in height of the Altiplano. This is consistent with expectations. First, a decrease in convergence rate should not accelerate surface uplift; instead such a decrease would more likely lead to a decrease in the rate of crustal thickening. By contrast, the removal of mantle lithosphere and its replacement by material of lower density not only leads to surface uplift, but also to an increase in the force per unit (horizontal) length that a high plateau applies to its

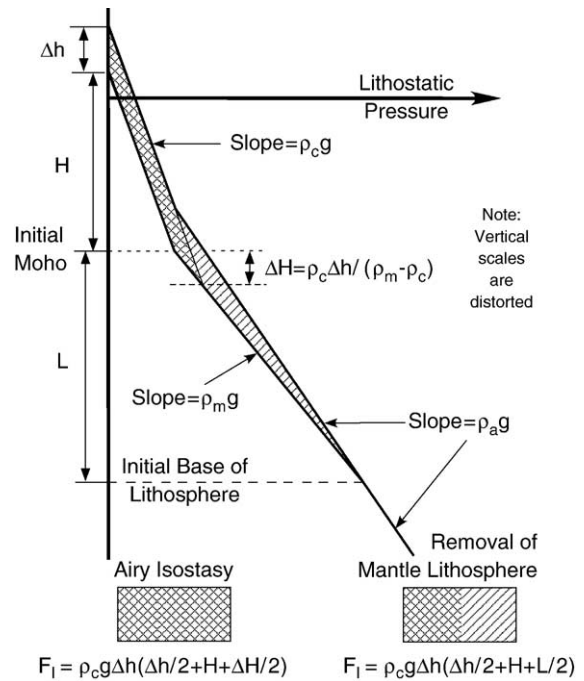


Fig. 7. Simplified plots of lithostatic pressure versus depth for different mechanisms responsible for an increase in mean elevation of Δh and resulting increases in force per unit length F_L that the high region applies to surrounding lowlands. Lithostatic pressure increases with depth with a gradient ρg , where ρ can be the density of crust ρ_c , mantle lithosphere ρ_m , or asthenosphere ρ_a , and g is gravity. Because ρ_c , ρ_m , and ρ_a differ little and the change in height Δh is a small fraction of the crustal thickness H , we have distorted the vertical axis to make the lines of different slopes and different positions clear. If the crust is thickened by an amount $\Delta H + \Delta h$, then because of Airy isostasy, the Moho deepens by $\Delta H = \Delta h \rho_c / (\rho_m - \rho_c) \approx 5.5 \Delta h$. The difference between integrated profiles of lithostatic pressure, equal to the area of cross hatching in the plot, gives the increase in force per unit length: $F_L = \rho_c \Delta h g (\Delta h/2 + H + \Delta H/2)$. If instead the surface rises because mantle lithosphere of mean density ρ_m is removed and replaced by less dense asthenosphere (ρ_a), then isostatic compensation yields the relationship: $\Delta h = L(\rho_m - \rho_c) / \rho_c$, where L is the initial thickness of mantle lithosphere. The area of both styles of hatching gives the increase in force per unit length: $F_L = \rho_c \Delta h g (\Delta h/2 + H + L/2)$. This shows that removal of mantle lithosphere leads to a large increase in the force per unit length applied to the surrounding regions.

surroundings, in this case the Nazca and South America plates.

8. Conclusions

Oxygen isotope paleoaltimetry of carbonates compared to elevation estimates from leaf physiognomy studies in the northern Altiplano demonstrates that the surface of the Andean plateau rapidly rose ~2.5 to 3.5 km between 10.3 and 6.8 Ma. The timing and magnitude of surface rise is consistent with numerous indicators that suggest that both the thermal structure of the lithosphere changed and surface uplift occurred at this time, including widespread incision of the San Juan del Oro paleosurface [19,24], increased rate of exhumation in the Eastern Cordillera [63], and eruption of mafic lavas beginning at ~7.5 Ma [18,33]. Several km of surface uplift in a period as short as 1 to 4 Myr requires the removal of mantle lithosphere, including an important component of eclogitic lower crust [4,6], and supports what has been a speculative suggestion that such mantle dynamics occur. This event also corresponds with a 30% decrease in the rate of convergence between the Nazca and South America plates as well as the propagation of the Andean fold-thrust belt into the Subandean zone. By inference, mantle dynamics beneath mountain belts appears to have a profound effect on both plate motions and the structural evolution of fold-thrust belts.

Acknowledgements

We thank D. Dettman, P. Higgins, K. Kodama, Z. Wallace, and S. Withers for lab assistance. S. Duzlak, R. Madoff, A. Rhodes-Golden, and J. Stern are thanked for assistance in the field. We are grateful to R. Allmendinger, J. Eiler, P. Ghosh, G. Hoke, S. Kay, and N. McQuarrie for valuable discussions, and C. P. Chamberlain, P. England, T. Jordan, and M. J. Kohn for constructive comments on the manuscript. This research has been supported by the National Science Foundation mostly through EAR (0230232) to Garzzone and EAR (0350396) Libarkin, and Molnar acknowledges support from EAR (0106909). Any opinions, findings, and conclusions or recommendations expressed in this material are those of the authors and do not necessarily reflect the views of the National Science Foundation.

References

- [1] R. Gonfiantini, M.-A. Roche, J.-C. Olivry, J.-C. Fontes, G.M. Zuppi, The altitude effect on the isotopic composition of tropical rains, *Chem. Geol.* 181 (2001) 147–167.
- [2] P. Bird, Initiation of intracontinental subduction in the Himalaya, *J. Geophys. Res.* 83 (B10) (1978) 4975–4987.
- [3] P.C. England, G. Houseman, Extension during continental convergence, with application to the Tibetan Plateau, *J. Geophys. Res.* 94 (B12) (1989) 17,561–17,579.
- [4] R.W. Kay, S. Mahlburg-Kay, Creation and destruction of lower continental crust, *Geol. Rundsch.* 80 (1991) 259–278.
- [5] K.D. Nelson, A unified view of craton evolution motivated by recent deep seismic reflection and refraction results, *Geophys. J. Int.* 105 (1) (1991) 25–35.
- [6] R.W. Kay, S.M. Kay, Delamination and delamination magmatism, *Tectonophysics* 219 (1993) 177–189.
- [7] J.F. Dewey, P.D. Ryan, T.B. Andersen, Orogenic uplift and collapse, crustal thickness, fabrics and metamorphic phase changes; the role of eclogites, in: H.M. Prichard, T. Alabaster, T.N.B.W. Harris, C.R. Neary (Eds.), *Magmatic Processes and Plate Tectonics*, Geological Society Special Publication, vol. 76, The Geological Society, London, 1993, pp. 325–343.
- [8] M.N. Ducea, J.B. Saleeby, Buoyancy sources for a large, unrooted mountain range, the Sierra Nevada, California; evidence from xenolith thermobarometry, *J. Geophys. Res.* 101 (4) (1996) 8229–8244.
- [9] M. Jull, P.B. Kelemen, On the conditions for lower crustal convective instability, *J. Geophys. Res.* 106 (4) (2001) 6423–6446.
- [10] P. Molnar, H. Lyon-Caen, Some simple physical aspects of the support, structure, and evolution of mountain belts, in: S.P. Clark, B.C. Burchfiel, J. Suppe (Eds.), *Processes in Continental Lithospheric Deformation*, *Geol. Soc. Amer. Spec. Pap.*, vol. 218, 1988, pp. 179–207.
- [11] B.K. Horton, B.A. Hampton, B.N. Lareau, E. Baldellon, Tertiary provenance history of the northern and central Altiplano (Central Andes, Bolivia); a detrital record of plateau-margin tectonics, *J. Sediment. Res.* 72 (5) (2002) 711–726.
- [12] D.S. Vandervoort, T.E. Jordan, P.K. Zeitler, R.N. Alonso, Chronology of internal drainage development and uplift, southern Puna Plateau, Argentine Central Andes, *Geology* 23 (2) (1995) 145–148.
- [13] P.G. DeCelles, B.K. Horton, Early to middle Tertiary foreland basin development and the history of Andean crustal shortening in Bolivia, *Geol. Soc. Amer. Bull.* 115 (1) (2003) 58–77.
- [14] J.P. Müller, J. Kley, V. Jacobshagen, Structure and Cenozoic kinematics of the Eastern Cordillera, southern Bolivia, *Tectonics* 21 (5) (2002), doi:10.1029/2001TC001340.
- [15] T. Sempere, G. Hérail, J. Oller, M.G. Bonhomme, Late Oligocene–early Miocene major tectonic crisis and related basins in Bolivia, *Geology* 18 (10) (1990) 946–949.
- [16] N. McQuarrie, The kinematic history of the Central Andean fold-thrust belt, Bolivia; implications for building a high plateau, *Geol. Soc. Amer. Bull.* 114 (8) (2002) 950–963.
- [17] J. Kley, Transition from basement-involved to thin-skinned thrusting in the Cordillera Oriental of southern Bolivia, *Tectonics* 15 (1996) 763–775.
- [18] S. Lamb, L. Hoke, Origin of the high plateau in the Central Andes, Bolivia, South America, *Tectonics* 16 (4) (1997) 623–649.
- [19] T.L. Gubbels, B.L. Isacks, E. Farrar, High-level surfaces, plateau uplift, and foreland development, Bolivian Central Andes, *Geology* 21 (8) (1993) 695–698.
- [20] I. Moretti, P. Baby, E. Mendez, D. Zubieta, Hydrocarbon generation in relation to thrusting in the Sub Andean zone from 18 to 22 degrees S, Bolivia, *Pet. Geosci.* 2 (1) (1996) 17–28.

- [21] L. Echavarría, R. Hernández, R. Allmendinger, J. Reynolds, Subandean thrust and fold belt of northwestern Argentina; geometry and timing of the Andean evolution, *AAPG Bull.* 87 (6) (2003) 965–985.
- [22] E. Kendrick, M. Bevis, S. Robert, B. Brooks, An integrated crustal velocity field for the Central Andes, *Geochem. Geophys. Geosyst.* 2 (2001), doi:10.1029/2001GC000191.
- [23] B.L. Isacks, Uplift of the Central Andean Plateau and bending of the Bolivian Orocline, *J. Geophys. Res.* 93 (4) (1988) 3211–3231.
- [24] L. Kennan, S.H. Lamb, L. Hoke, High-altitude palaeosurfaces in the Bolivian Andes; evidence for late Cenozoic surface uplift, in: M. Widdowson (Ed.), *Palaeosurfaces; Recognition, Reconstruction and Palaeoenvironmental Interpretation*, Geological Society Special Publication, vol. 120, The Geological Society, London, 1997, pp. 307–323. Geological Society of London.
- [25] T. Sempere, R.F. Butler, D.R. Richards, L.G. Marshall, W. Sharp, C.C. Swisher III, Stratigraphy and chronology of Upper Cretaceous–lower Paleogene strata in Bolivia and Northwest Argentina, *Geol. Soc. Amer. Bull.* 109 (6) (1997) 709–727.
- [26] K.M. Gregory-Wodzicki, Uplift history of the Central and Northern Andes; a review, *Geol. Soc. Amer. Bull.* 112 (7) (2000) 1091–1105.
- [27] K.M. Gregory-Wodzicki, W.C. McIntosh, K. Velasquez, Climatic and tectonic implications of the late Miocene Jakokkota Flora, Bolivian Altiplano, *J. South Am. Earth Sci.* 11 (6) (1998) 533–560.
- [28] X. Yuan, S.V. Sobolev, R. Kind, Moho topography in the Central Andes and its geodynamic implications, *Earth Planet. Sci. Lett.* 199 (3–4) (2002) 389–402.
- [29] S.L. Beck, G. Zandt, The nature of orogenic crust in the Central Andes, *J. Geophys. Res.* 107 (2002), doi:10.1029/2000JB000124.
- [30] C. Dorbath, M. Granet, Local earthquake tomography of the Altiplano and Eastern Cordillera of northern Bolivia, *Tectonophysics* 259 (1996) 117–136.
- [31] S. Myers, S. Beck, G. Zandt, T. Wallace, Lithospheric-scale structure across the Bolivian Andes from tomographic images of velocity and attenuation for P and S waves, *J. Geophys. Res.* 103 (1998) 21233–21252.
- [32] L. Hoke, D.R. Hilton, S.H. Lamb, K. Hammerschmidt, H. Friedrichsen, ^3He evidence for a wide zone of active mantle melting beneath the Central Andes, *Earth Planet. Sci. Lett.* 128 (3–4) (1994) 341–355.
- [33] G. Carlier, J.P. Lorand, J.P. Liégeois, M. Fornari, P. Soler, V. Carlotto, J. Cárdenas, Potassic–ultrapotassic mafic rocks delineate two lithospheric mantle blocks beneath the southern Peruvian Altiplano, *Geology* 33 (2005) 601–604.
- [34] S.M. Kay, B. Coira, J. Viramonte, Young mafic back arc volcanic rocks as indicators of continental lithospheric delamination beneath the Argentine Puna Plateau, Central Andes, *J. Geophys. Res.* 99 (12) (1994) 24323–24339.
- [35] J.G. Masek, B.L. Isacks, T.L. Gubbels, E.J. Fielding, Erosion and tectonics at the margins of continental plateaus, *J. Geophys. Res.* 99 (7) (1994) 13941–13956.
- [36] D.R. Montgomery, G. Balco, S.D. Willett, Climate, tectonics, and the morphology of the Andes, *Geology* 29 (7) (2001) 579–582.
- [37] R. Garreaud, M. Vuille, A.C. Clement, The climate of the Altiplano; observed current conditions and mechanisms of past changes, *Palaeogeogr. Palaeoclimatol. Palaeoecol.* 194 (2003) 5–22.
- [38] M. Vuille, R.S. Bradley, M. Werner, R. Healy, F. Keimig, Modeling $\delta^{18}\text{O}$ in precipitation over the tropical Americas: 1. Interannual variability and climatic controls, *J. Geophys. Res.* 108 (2003), doi:10.1029/2001JD002038.
- [39] C.N. Alpers, G.H. Brimhall, Middle Miocene climatic change in the Atacama Desert, northern Chile; evidence from supergene mineralization at La Escondida, *Geol. Soc. Amer. Bull.* 100 (10) (1988) 1640–1656.
- [40] G.D. Hoke, B.L. Isacks, T.E. Jordan, J.S. Yu, Groundwater-sapping origin for the giant quebradas of northern Chile, *Geology* 32 (7) (2004) 605–608.
- [41] B.K. Horton, Erosional control on the geometry and kinematics of thrust belt development in the Central Andes, *Tectonics* 18 (6) (1999) 1292–1304.
- [42] P. Roperch, G. Herail, M. Fornari, Magnetostratigraphy of the Miocene Corque Basin, Bolivia; implications for the geodynamic evolution of the Altiplano during the late Tertiary, *J. Geophys. Res.* 104 (9) (1999) 20415–20429.
- [43] L.G. Marshall, C.C. Swisher III, A. Lavenu, R. Hoffstetter, G.H. Curtis, Geochronology of the mammal-bearing late Cenozoic on the northern Altiplano, Bolivia, *J. South Am. Earth Sci.* 5 (1) (1992) 1–19.
- [44] P., Ghosh, C.N., Garziona, J.M., Eiler, Rapid uplift of the Altiplano revealed in ^{13}C – ^{18}O bonds in paleosol carbonates, *Science*, in press.
- [45] E.H. Lindsay, Mammalian chronology and the magnetic polarity time scale, in: M.O. Woodburne (Ed.), *Cenozoic Mammals of North America*, Univ. Calif. Press, Berkeley, 1987, pp. 269–284.
- [46] G.H. Mack, D.R. Cole, L. Trevino, The distribution and discrimination of shallow, authigenic carbonate in the Pliocene–Pleistocene Palomas Basin, southern Rio Grande Rift, *Geol. Soc. Amer. Bull.* 112 (5) (2000) 643–656.
- [47] U. Siegenthaler, H. Oeschger, Correlation of ^{18}O in precipitation with temperature and altitude, *Nature* 285 (1980) 314–317.
- [48] C.N. Garziona, J. Quade, P.G. DeCelles, N.B. English, Predicting paleoelevation of Tibet and the Himalaya from $\delta^{18}\text{O}$ vs. altitude gradients in meteoric water across the Nepal Himalaya, *Earth Planet. Sci. Lett.* 183 (1–2) (2000) 215–229.
- [49] D.B. Rowley, R.T. Pierrehumbert, B.S. Currie, A new approach to stable isotope-based paleoaltimetry; implications for paleoaltimetry and paleohypsometry of the High Himalaya since the late Miocene, *Earth Planet. Sci. Lett.* 188 (1–2) (2001) 253–268.
- [50] M.A. Poage, C.P. Chamberlain, Empirical relationships between elevation and the stable isotope composition of precipitation and surface waters; considerations for studies of paleoelevation change, *Am. J. Sci.* 301 (1) (2001) 1–15.
- [51] C.N. Drummond, B.H. Wilkinson, K.C. Lohmann, G.R. Smith, Effect of regional topography and hydrology on the lacustrine isotopic record of Miocene paleoclimate in the Rocky Mountains, *Palaeogeogr. Palaeoclimatol. Palaeoecol.* 101 (1–2) (1993) 67–79.
- [52] D.L. Dettman, K.C. Lohmann, Oxygen isotope evidence for high-altitude snow in the Laramide Rocky Mountains of North America during the Late Cretaceous and Paleogene, *Geology* 28 (3) (2000) 243–246.
- [53] C.N. Garziona, D.L. Dettman, J. Quade, P.G. DeCelles, R.F. Butler, High times on the Tibetan Plateau; paleoelevation of the Thakkhola Graben, Nepal, *Geology* 28 (4) (2000) 339–342.

- [54] S.-T. Kim, J.R. O'Neil, Equilibrium and nonequilibrium oxygen isotope effects in synthetic carbonates, *Geochim. Cosmochim. Acta* 61 (16) (1997) 3461–3475.
- [55] B.B. Wolfe, R. Aravena, M.B. Abbott, G.O. Seltzer, J.J. Gibson, Reconstruction of paleohydrology and paleohumidity from oxygen isotope records in the Bolivian Andes, *Palaeogeogr. Palaeoclimatol. Palaeoecol.* 176 (1–4) (2001) 177–192.
- [56] P. Ghosh, J. Adkins, H. Affek, B. Balta, W. Guo, E.A. Schauble, D. Schrag, J.M. Eiler, ^{13}C - ^{18}O bonds in carbonate minerals: a new kind of paleothermometer, *Geochim. Cosmochim. Acta*, in press.
- [57] B.M. Sheffels, Lower bound on the amount of crustal shortening in the central Bolivian Andes, *Geology* 18 (9) (1990) 812–815.
- [58] D. Hindle, J. Kley, O. Oncken, S. Sobolev, Crustal balance and crustal flux from shortening estimates in the Central Andes, *Earth Planet. Sci. Lett.* 230 (2005) 113–124.
- [59] G.A. Houseman, D.P. McKenzie, P. Molnar, Convective instability of a thickened boundary layer and its relevance for the thermal evolution of continental convergent belts, *J. Geophys. Res.* 86 (7) (1981) 6115–6132.
- [60] L.M. Cathles III, *The Viscosity of the Earth's Mantle*, Princeton Univ. Press, Princeton, N.J., 1975, 386 pp.
- [61] J.-M. Nocquet, E. Calais, B. Parsons, Geodetic constraints on glacial isostatic adjustment in Europe, *Geophys. Res. Lett.* 32 (2005), doi:10.1029/2004GL022174.
- [62] B.G. Bills, S.L. de Silva, D.R. Curry, R.S. Emenger, K.D. Lillquist, A. Donnellan, B. Worden, Hydro-isostatic deflection and tectonic tilting in the Central Andes; initial results of a GPS survey of Lake Minchin shorelines, *Geophys. Res. Lett.* 21 (4) (1994) 293–296.
- [63] R.J. Gillis, B.K. Horton, M. Grove, Exhumation history and basin development along the eastern margin of the central Andean Plateau, Bolivia, *Abstr. Programs - Geol. Soc. Am.* 36 (5) (2004) 433.
- [64] K. Elger, O. Oncken, J. Glodny, Plateau-style accumulation of deformation: Southern Altiplano, *Tectonics* 24 (2005), doi:10.1029/2004TC001675.
- [65] R.W. Allmendinger, T.E. Jordan, S.M. Kay, B.L. Isacks, The evolution of the Altiplano–Puna Plateau of the Central Andes, *Annu. Rev. Earth Planet. Sci.* 25 (1997) 139–174.
- [66] D. Davis, J. Suppe, F.A. Dahlen, Mechanics of fold-and-thrust belts and accretionary wedges, *J. Geophys. Res.* 88 (2) (1983) 1153–1172.
- [67] F.A. Dahlen, Noncohesive critical Coulomb wedges; an exact solution, *J. Geophys. Res.* 89 (B12) (1984) 10125–10133.
- [68] P.G. DeCelles, G. Mitra, History of the Sevier orogenic wedge in terms of critical taper models, Northeast Utah and Southwest Wyoming, *Geol. Soc. Amer. Bull.* 107 (4) (1995) 454–462.
- [69] S.C. Cande, J.L. LaBrecque, W.F. Haxby, Plate kinematics of the South Atlantic; Chron C34 to present, *J. Geophys. Res.* 93 (11) (1988) 13479–13492.
- [70] S.F. Tebbens, S.C. Cande, Southeast Pacific tectonic evolution from early Oligocene to present, *J. Geophys. Res.* 102 (6) (1997) 12061–12084.
- [71] P. Molnar, P. England, J. Martinod, Mantle dynamics, uplift of the Tibetan Plateau, and the Indian monsoon, *Rev. Geophys.* 31 (4) (1993) 357–396.
- [72] F.C. Frank, Plate tectonics, the analogy with glacier flow, and isostasy, *Flow and Fracture of Rock*, The Griggs Volume, Geophysical Monograph, vol. 16, Am Geophys. Un., Washington, D.C., 1972, pp. 285–292.
- [73] D.P. McKenzie, Plate tectonics, in: E.C. Robertson (Ed.), *The Nature of the Solid Earth*, McGraw-Hill, New York, NY, 1972, pp. 323–360.
- [74] T.E. Jordan, B.L. Isacks, R.W. Allmendinger, J.A. Brewer, V.A. Ramos, C.J. Ando, Andean tectonics related to geometry of subducted Nazca Plate, *Geol. Soc. Amer. Bull.* 94 (3) (1983) 341–361.
- [75] S.C. Cande, D.V. Kent, Revised calibration of the geomagnetic polarity timescale for the Late Cretaceous and Cenozoic, *J. Geophys. Res.* 100 (4) (1995) 6093–6095.
- [76] D. Chu, R.G. Gordon, Evidence for motion between Nubia and Somalia along the Southwest Indian Ridge, *Nature* 398 (1999) 64–67.
- [77] J. Lemaux II, R.G. Gordon, J.-Y. Royer, Location of the Nubia–Somalia boundary along the Southwest Indian Ridge, *Geology* 30 (4) (2002) 339–342.
- [78] J.-Y. Royer, T. Chang, Evidence for relative motions between the Indian and Australian plates during the last 20 m.y. from plate tectonic reconstructions; implications for the deformation of the Indo-Australian Plate, *J. Geophys. Res.* 96 (7) (1991) 11779–11802.
- [79] S.C. Cande, J.M. Stock, Pacific–Antarctic–Australia motion and the formation of the Macquarie Plate, *Geophys. J. Int.* 157 (1) (2004) 399–414.
- [80] S.C. Cande, D.V. Kent, A new geomagnetic polarity time scale for the Late Cretaceous and Cenozoic, *J. Geophys. Res.* 97 (10) (1992) 13917–13951.
- [81] F. Pardo-Casas, P. Molnar, Relative motion of the Nazca (Farallon) and South American plates since Late Cretaceous time, *Tectonics* 6 (3) (1987) 233–248.